

Do transient gravity waves in a shear flow break?

M. Pulido* and C. Rodas

Department of Physics, FACENA, Universidad Nacional del Nordeste, Argentina

ABSTRACT: The propagation of transient gravity waves in a shear flow towards their critical levels is examined using a ray tracing approximation and a higher-degree (quasi-optic) approximation. Because of its transient forcing, the amplitude of transient waves decays to zero in the neighbourhood of the critical region so that it is not clear whether transient gravity waves will reach the convective instability threshold or not. The analysis shows that the horizontal perturbation decays asymptotically as the inverse of the square root of time, while the vertical wavenumber depends linearly on time, thus transient gravity waves attain convective instability for long times. The theoretical results are compared with numerical simulations. The ray path approximation is not able to reproduce the maximum amplitude, but the quasi-optic approximation gives a reasonable agreement at short and long times. There are three breaking regimes for transient gravity waves. For wave packets with a narrow frequency spectrum (quasi-steady waves) and large enough initial wave amplitude, the wave breaking is similar to the abrupt monochromatic wave overturning. On the other hand, highly transient wave packets will dissipate near the critical region for very long times with small wave amplitudes and high vertical wavenumber. The third regime is a transition between the two extremes; in this case both wave amplitude and vertical wavenumber are important to produce the convective threshold. The dependencies of the convective instability height (a quantity that may be useful for gravity wave parametrizations) on the Richardson number and the frequency spectral width are obtained. Copyright © 2008 Royal Meteorological Society

KEY WORDS convective instability; quasi-optics; gravity wave parametrizations; wave breaking; ray tracing

Received 16 November 2007; Revised 16 April 2008; Accepted 9 May 2008

1. Introduction

Gravity waves interact continuously with the mean flow where they propagate. Sometimes the mean flow feeds energy and momentum into the wave field and sometimes otherwise. These interactions may be reversible during conservative propagation and irreversible during gravity wave dissipation. One of the most effective mechanisms of dissipation of internal gravity waves in the atmosphere is their convective overturning (Fritts, 1984). This occurs when the amplitude of the wave exceeds a threshold so that the wave-induced potential temperature produces a local decrease of potential temperature with height and therefore a convective instability. Above this threshold the dynamics are expected to be dominated by nonlinearities, the gravity wave starts breaking and its momentum is deposited in the mean flow.

The irreversible forcing produced by gravity waves on the mean flow is responsible for changes in the meridional circulation from the troposphere (Palmer *et al.*, 1986) to the mesosphere (Holton, 1982). At that height the gravity wave drag is believed to produce the meridional circulation that inverts the meridional temperature gradient. This gravity wave drag is accounted for by parametrizations in general circulation models.

A steady-state wave in a horizontal background flow that depends on height conserves its vertical momentum flux (Lighthill, 1978). If the wave possess a critical level, wave energy density diverges and the wave is strongly attenuated at the critical level, so that there is no sign of the wave above the critical level assuming a background flow with large Richardson number (Booker and Bretherton, 1967). Actually, a dissipative mechanism via nonlinear processes or viscosity must be activated before the wave reaches the critical level. Brown and Stewartson (1980) further extended the Booker and Bretherton analysis by considering nonlinear processes inside the critical layer and linear theory outside it; they found that the reflection coefficient increases with time.

Transient gravity waves do not conserve vertical momentum flux as they propagate towards the critical region. The amplitude evolution is governed by the wave action conservation equation (Bretherton and Garrett, 1968). This fact introduces notable differences; while the wave energy density of steady-state waves (whose vertical momentum flux is constant below the critical level) increases indefinitely in the neighbourhood of the critical level, for transient waves the wave energy density decreases. This difference is also present in the spectral evolution; a m^{-1} power law is satisfied for steady-state waves since vertical momentum flux is constant with height (Hines, 1991). In the case of transient gravity waves, the spectral evolution is governed by a m^{-3} power

*Correspondence to: M. Pulido, Department of Physics, FACENA, Universidad Nacional del Nordeste, Av. Libertad 5400, (3400) Corrientes, Argentina. E-mail: pulido@unne.edu.ar

law which is a consequence of wave action conservation (Pulido, 2005).

The propagation of a gravity wave packet in a shear flow was examined by Grimshaw (1975) through numerical simulations. He focused on the nonlinear interactions between the background flow and the wave packet using the wave action conservation equation and the horizontal momentum equation of the background flow. His small initial amplitude analysis closely resembles the present study, however there is a key point where they differ: Grimshaw (1975) assumes that all the components of the wave packet have a fixed absolute frequency so that the wave action density does not depend on time. A consequence of this assumption is that the wave packet vertical width goes to zero as time goes on, so that wave energy density increases indefinitely in the neighbourhood of the critical level in the absence of dissipation. In the present work we examine a wave packet with a frequency distribution so that the wave action density does depend on time.

Considering the irreversible feedback processes between the wave field and the mean flow that take place in the atmosphere, transient gravity wave momentum deposition may produce responses in the general circulation that are not necessarily reproduced by steady-state wave momentum deposition. The effects of gravity wave pulses in the equatorial stratosphere were examined by Piani *et al.* (2004). They found that the deposited gravity wave momentum is larger in the vertical width of interest when a stochastic gravity wave parametrization is used. It was shown that this parametrization gives a more realistic quasi-biennial oscillation in multidecadal simulations.

Jones (1967) examined gravity waves propagating on a shear flow in a rotating frame. There are three singularities in this case, one of which is the critical level and the other two levels are located where the magnitude of the intrinsic frequency equals the Coriolis frequency. These inertia critical levels depend on the horizontal wavenumber, so that a disturbance that is composed of a continuous distribution in the horizontal wavenumber and a fixed absolute frequency possesses a different inertia critical level for each component. This effect was examined by Wurtele *et al.* (1996) who found through numerical experiments that the amplitude of an orographic wave spectrum remains finite and the evolution of broad horizontal wavenumber spectra appears to be dominated by linear processes. On the other hand, nonlinear processes are found for narrow spectra.

Shutts (1998) and Broad (1999) examined a spectrum of orographic waves propagating in a horizontal background wind that is rotating with height. In this case there is also a different critical level for each component. They found that the wave energy density does not increase indefinitely but decays to zero along the ray path. However, the vertical wavenumber becomes unbounded at a critical level, so that the existence of the convective overturning depends on the asymptotic tendencies. Broad

(1999) found that the vertical wavenumber increase dominates the vertical shear so that the convective threshold is exceeded in the neighbourhood of the critical level.

For a transient gravity wave propagating in a wind shear, each component (of the frequency spectrum in this case) possesses its own critical level as indicated by the cases examined by Shutts (1998), Broad (1999) and Wurtele *et al.* (1996). The critical region is the vertical width over which each component of the wave spectrum finds its critical level; this vertical width will depend on the width of the horizontal phase speed spectrum and the vertical shear of the horizontal background wind. As the forcing is transient, we expect that wave energy (and so the wave amplitude) goes to zero at the critical region. The instability threshold will depend on the value of the amplitude and the vertical wavelength. Since vertical wavelength also decreases, the asymptotic behaviour of amplitude and vertical wavelength for long times will determine whether the instability threshold is reached. This is one of the purposes of this work, to determine whether a transient gravity wave in a shear flow will attain convective instability when it propagates towards the critical region.

Another objective of this work is to compare numerical simulations of the wave amplitude evolution with the theoretical results obtained using ray tracing and a higher-degree approximation. Although the asymptotic behaviour for long times is well captured by the ray tracing approximation, we find important differences for shorter times; in particular, we find a characteristic maximum in the wave amplitude which is not predicted by the ray tracing approximation. The proposed higher-degree approximation (known as quasi-optics) shows good agreement with numerical simulations at short and long times.

2. Ray tracing

Consider waves which are small perturbations to a basic state which is characterised by a zonal wind $u_0(z)$ and a constant buoyancy frequency N_0 . We neglect rotation and viscosity effects and take the hydrostatic and WKB approximations. The resulting dispersion relation is

$$\omega = ku_0(z) \pm \frac{N_0 k}{m}, \quad (1)$$

where ω is the absolute frequency, k is the horizontal wavenumber and m the height-dependent vertical wavenumber.

We assume a wave packet with a fixed horizontal wavenumber, k_f , a frequency distribution localised around a central frequency ω_c and with a spectral width of $\Delta\omega$. By means of the dispersion relation (1), the frequency distribution results in a vertical wavenumber distribution which is centred at $m(\omega_c)$.

The trajectory of a gravity wave packet is given by

$$d_t x = \partial_k \omega = u_0(z) - \frac{N_0}{m}, \quad d_t z = \partial_m \omega = \frac{N_0 k_f}{m^2}. \quad (2)$$

Since we consider waves that are propagating upward, we have kept the negative sign in (1).

If at time $t = 0$ the packet is located at (x_i, z_i) then from (2),

$$x - x_i = \frac{\omega}{k_f}t, \quad t = N_0 k_f \int_{z_i}^z \frac{dz'}{\{\omega - k_f u_0(z')\}^2}. \quad (3)$$

Equation (3) yields the trajectory $(x, z) = (x(\omega, t), z(\omega, t))$ for the wave packet with central frequency ω .

The energy of the wave packet is governed by the wave action conservation equation (Bretherton and Garrett, 1968),

$$\partial_t \left(\frac{W_r}{\Omega} \right) + \nabla \cdot \left(\mathbf{c}_g \frac{W_r}{\Omega} \right) = 0, \quad (4)$$

where W_r is the wave energy density, $\Omega = \omega - k u_0$ is the intrinsic frequency and $\mathbf{c}_g = (\partial_k \omega, \partial_m \omega)$ is the group velocity.

Integrating in height in a vertical interval long enough to contain the whole disturbance, (4) results in

$$\partial_t \int_0^\infty \frac{W_r}{\Omega(z')} dz' = 0. \quad (5)$$

The wave energy density is uniform in the horizontal coordinate so that W_r is given per horizontal distance unit.

As we consider a wave packet, it is localised in a limited region with a vertical width Δz ; the wave energy density outside this vertical width is considered negligible (e.g. Broad, 1999),

$$\frac{\langle W_r \rangle(t)}{\Omega} \Delta z = \frac{\langle W_r \rangle(0)}{\Omega_i} \Delta z_i, \quad (6)$$

where Δz_i is the vertical width at the initial time, $\langle \cdot \rangle$ means an average within the vertical width, and Ω_i is the intrinsic frequency of the central mode at the initial time.

Using the principle of energy equipartition and considering quasi-horizontal movements, the wave energy density is given by (e.g. Pulido, 2005)

$$W_r = \overline{\rho_0 u_1^2}, \quad (7)$$

where u_1 is the horizontal wind perturbation induced by the wave and the overline means a phase average of the field.

We focus on the gravity wave breaking process induced by gravity wave – mean flow interactions so that the density decrease in height is neglected. Therefore the background density is considered constant. From (6) and (7), the evolution of the envelope amplitude $a(t) = \sqrt{\overline{u_1^2}}$ becomes

$$a(t) = a(0) \sqrt{\frac{\Omega(t) \Delta z_i}{\Omega_i \Delta z}}. \quad (8)$$

The evolution of the wave packet vertical width (which forms the so-called ray tube) is related to the spectral

width through the Jacobian of the transformation between the physical and spectral space (Broad, 1999):

$$\Delta z = (\partial_\omega z)_{\omega=\omega_c} \Delta \omega. \quad (9)$$

The Jacobian is determined using the ray tracing equation ($z = z(\omega, t)$). The transformation is represented as a function of absolute frequency so that the spectral width, $\Delta \omega$, is constant along the ray. On the other hand, the vertical wavenumber range will not necessarily be constant, except for a linear background wind where the vertical wavenumber range is constant in time although the vertical wavenumber does depend linearly on time.

Furthermore, the initial vertical width Δz_i may be expressed in the frequency spectrum, $\Delta z_i = (\partial_m \omega)_{t=t_i} \Delta t_i$. From Fourier analysis we use the well-known relationship $\Delta t_i = \Delta \omega^{-1}$, so the initial vertical width may be expressed as

$$\Delta z_i = \frac{\omega_c^2}{N_0 k_f \Delta \omega}. \quad (10)$$

Hence, the resulting amplitude evolution yields

$$a(t) = a(0) \sqrt{\frac{\Omega(t)}{\Omega_i} \frac{\omega_c^2}{N_0 k_f \Delta \omega^2} (\partial_\omega z)^{-1}}. \quad (11)$$

2.1. Wave amplitude evolution in a linear horizontal wind

In the general case, the trajectory and amplitude can be determined through a numerical integration of (3) and (9). To evaluate the tendencies in a particular case we assume a linear horizontal background wind, i.e. $U(z) = d_z U z$, where $d_z U$ is constant. In this case calculations can be carried out analytically.

From (1) and (3), the trajectory yields

$$z(\omega, t) = \frac{\omega^2 t}{k_f N_0 (1 + Ri^{-1/2} \omega t)}, \quad (12)$$

where the background Richardson number is $Ri = N_0^2 / (\partial_z u_0)^2$. We assume that at the initial time $t = 0$ the wave packet is at the origin $(x, z) = (0, 0)$.

From (12), as $t \rightarrow \infty$, the height of the wave packet with central frequency ω_c tends to $\omega_c / (d_z U k_f) = z_c$, where z_c is the critical level of the central frequency.

The Jacobian of the transformation for the central frequency of the packet in the neighbourhood of the critical region is

$$\partial_\omega z |_{\omega_c} = \frac{\omega_c t}{k_f N_0} \frac{2 + Ri^{-1/2} \omega_c t}{(1 + Ri^{-1/2} \omega_c t)^2}. \quad (13)$$

Replacing (13) in (11), the amplitude of the wave packet is

$$a(t) = a(0) \sqrt{\frac{\omega_c}{\Delta \omega^2 t} \frac{1 + Ri^{-1/2} \omega_c t}{2 + Ri^{-1/2} \omega_c t}}. \quad (14)$$

As expected, when $t \rightarrow 0$, all the rays converge at the initial point $(0, 0)$ and therefore the amplitude goes to infinity.

For long times the amplitude in a wave packet that is propagating towards the critical region goes to zero; it diminishes as $t^{-1/2}$. This behaviour is in contrast with monochromatic waves whose amplitudes diverge at the critical level. Modes that compose the wave packet are interfering destructively in the neighbourhood of the critical region. However, this does not mean that the wave will not break; the vertical wavenumber increases as time goes on so the asymptotic tendency of the vertical shear of the horizontal perturbation, $\partial_z u_1$, is not evident. This is examined in section 4.

The wave energy density is proportional to the square of the amplitude (7), so it diminishes as t^{-1} for long times. This result reminds us of the steady-state case examined by Broad (1999), where an orographic wave propagates in a flow in which the wind direction is turning with height. For a broad wavenumber spectrum, there are multiple critical levels where $\mathbf{U} \cdot \mathbf{k} = 0$, in which case the wave energy density also goes to zero. It goes as $(z - z_c)$ at the so-called 3D critical levels. Because it is a steady-state case, the analysis is done for altitude tendencies instead of time tendencies.

3. Quasi-optic approximation

The ray tracing approximation assumes that the wave packet is concentrated in a point at the initial time so that this approximation can only be used for long times. In other words, result (14) gives the dominant terms of the asymptotic expansion for long times. (Note that the ray path is not strictly the asymptotic term.) However we expect that the wave packet achieves a maximum amplitude and after that the amplitude starts to decay, a feature that is not captured by the ray path approximation. A better approximation is needed to determine whether the wave packet reaches the convective instability threshold before the maximum amplitude or before the maximum vertical wavenumber, namely near the critical level. In this work we apply the quasi-optic approximation which keeps information about the initial width of the wave packet. This approximation is usually found in quantum mechanics books to explain in classical terms the growing uncertainty in position as the wave packet spreads. A general introduction to the quasi-optic approximation may be found in Ostrovsky and Potapov (1999).

Since the background fields are independent of both time and horizontal coordinate, the general solution under the WKB approximation may be written as

$$u(x, z, t) = \frac{1}{\sqrt{2\pi}} \int \widehat{u}(\omega) \left\{ \frac{m(\omega, z)}{m(\omega, z_i)} \right\}^{1/2} \exp(i\psi) d\omega, \tag{15}$$

where $m(\omega, z)$ is given by (1) and the phase is defined as

$$\psi = \omega t - k_f x + \int_{z_i}^z m(\omega, z') dz'. \tag{16}$$

As in the ray tracing approximation, the horizontal wavenumber is fixed to be k_f .

The solution (15) is expressed as a Fourier integral in absolute frequency because this parameter is constant along the propagation and therefore the frequency spectrum, $\widehat{u}(\omega)$, does not evolve with time. (This is a key point in the proof; any attempt to work with the vertical wavenumber would be fruitless because of refraction (Pulido, 2005).)

We assume a Gaussian frequency spectrum with central frequency ω_c and spectral width σ_ω ,

$$\widehat{u}(\omega) = \frac{\widehat{u}_\omega}{\sigma_\omega} \exp \left\{ -\frac{(\omega - \omega_c)^2}{2\sigma_\omega^2} \right\}. \tag{17}$$

The phase ψ is expanded in Taylor series up to second order in ω around the central frequency and the amplitude term is expanded only up to first order in (15). This is done assuming a large Richardson number, an assumption consistent with the WKB approximation. This assumption implies that the amplitude term changes are slower than the oscillatory term changes, so that it is only necessary to retain the first order in the amplitude expansion. The resulting integral is

$$u = \frac{\widehat{u}_\omega}{\sqrt{2\pi}\sigma_\omega} \left(\frac{m_c}{m_{ic}} \right)^{1/2} \exp(i\psi_c) \times \int_{-\infty}^{\infty} \exp \left\{ -\frac{(\omega - \omega_c)^2}{2\sigma_\omega^2} \right\} \times \exp \left[i \left\{ \partial_\omega \psi_c (\omega - \omega_c) + \frac{1}{2} \partial_{\omega\omega}^2 \psi_c (\omega - \omega_c)^2 \right\} \right] d\omega. \tag{18}$$

The subscript c means evaluation at $\omega = \omega_c$.

Expression (18) is then integrated by completing squares in the exponents. The result is

$$u = \frac{\widehat{u}_\omega}{\sigma_\omega} \left(\frac{m_c}{m_{ic}} \right)^{1/2} \frac{\exp\{i(\psi_c - \theta/2)\}}{\{1/\sigma_\omega^4 + (\partial_{\omega\omega}^2 \psi_c)^2\}^{1/4}} \times \exp \left\{ -\frac{(\partial_\omega \psi_c)^2}{2(\sigma_\omega^{-2} - i\partial_{\omega\omega}^2 \psi_c)} \right\}, \tag{19}$$

where $\theta = \tan^{-1}(-\partial_{\omega\omega}^2 \psi_c \sigma_\omega^2)$. The exponential with imaginary argument represents the phase of the principal component, and the real exponential is the modulation of the amplitude that propagates with the group velocity

$$\partial_\omega \psi_c = 0. \tag{20}$$

Equation (20) defines the path of the central mode.

The limit case for $1/\sigma_\omega \rightarrow 0$ resembles the phase of the stationary phase method: $\theta/2 = \pi/4$ or $3\pi/4$. These are related to the slopes of the steepest descent path in the integration near a stationary point (Lighthill, 1978).

The amplitude of the envelope is

$$a(t) = \hat{u}_\omega \left(\frac{m_c}{m_{ic}} \right)^{1/2} \{ 1 + \sigma_\omega^4 (\partial_{\omega\omega}^2 \psi_c)^2 \}^{-1/4}. \quad (21)$$

Here the amplitude evolution is not only given by the vertical wavenumber square root dependencies but also by the second derivative of the phase which represents the dispersion of the wave packet. Wave energy density diminishes because ray paths with different absolute frequencies separate. Contrary to ray tracing, in this approximation the amplitude of the Gaussian packet always remains finite even at the initial time where $\partial_{\omega\omega}^2 \psi_c(t=0) = 0$ and then $a(t=0) = \hat{u}_\omega$.

For the limit $\sigma_\omega \rightarrow 0$, the monochromatic amplitude is recovered from (21)

$$a_{\sigma_\omega \rightarrow 0} = \hat{u}_\omega \left(\frac{m_c}{m_{ic}} \right)^{1/2}, \quad (22)$$

and therefore $a_{\sigma_\omega \rightarrow 0}$ is unbounded in the neighbourhood of the critical level because $m_c \rightarrow \infty$ at that level. On the other hand, the broader the frequency spectrum, the smaller the amplitude, from (21), because of dispersion.

The solution given by the quasi-optic approximation (19) not only gives the evolution of wave amplitude but also determines the evolution of the wave packet temporal range; using $\Delta z = \partial_m \omega \Delta t$, the vertical width is

$$\Delta z = \Delta z_i \left(\frac{m_{ic}}{m_c} \right)^2 \{ 1 + \sigma_\omega^4 (\partial_{\omega\omega}^2 \psi_c)^2 \}^{1/2}. \quad (23)$$

3.1. Wave amplitude evolution in a linear horizontal wind

The propagation of a Gaussian wave packet in a linear background wind (the same conditions as section 2.1) is an example where the evolution of the wave packet can be examined analytically under the quasi-optic approximation.

The first derivative of the phase, (16), is given by

$$\partial_\omega \psi_c = t - \frac{N_0 k_f z}{(1 - z/z_c) \omega_c^2}. \quad (24)$$

From the stationary phase condition, $\partial_\omega \psi_c = 0$, the ray equation (12) results. Using (24) and (12), the dispersion of the waves with different frequencies for a linear background wind yields

$$\partial_{\omega\omega}^2 \psi_c = \frac{t}{\omega_c} (2 + Ri^{-1/2} \omega_c t). \quad (25)$$

Therefore the vertical width of the wave packet increases as the wave packet propagates towards the critical region.

The vertical wavenumber from (1) and (12) is expected to grow in the form

$$\left(\frac{m_c}{m_{ic}} \right) = (1 + Ri^{-1/2} \omega_c t). \quad (26)$$

Finally, replacing (25) and (26) in (21) results in

$$a = \frac{\hat{u}_\omega}{\sigma_\omega} \frac{(1 + Ri^{-1/2} \omega_c t)^{1/2}}{\{ 1/\sigma_\omega^4 + (t/\omega_c)^2 (2 + Ri^{-1/2} \omega_c t)^2 \}^{1/4}}. \quad (27)$$

A comparison between the amplitude evolution given by the quasi-optic approximation, (27), with the amplitude evolution given by ray path approximation is shown in Figure 3 (continuous and dashed curves respectively). The quasi-optic approximation can capture the finite initial amplitude, then the amplitude presents a maximum and finally the asymptotic behaviour is achieved. In contrast, the amplitude under the ray path approximation is unbounded at the initial time and then diminishes monotonically.

The asymptotic term of (27) for long times is

$$a_{t \rightarrow \infty} = \frac{\hat{u}_\omega}{\sigma_\omega} \left(\frac{\omega_c}{t} \right)^{1/2}. \quad (28)$$

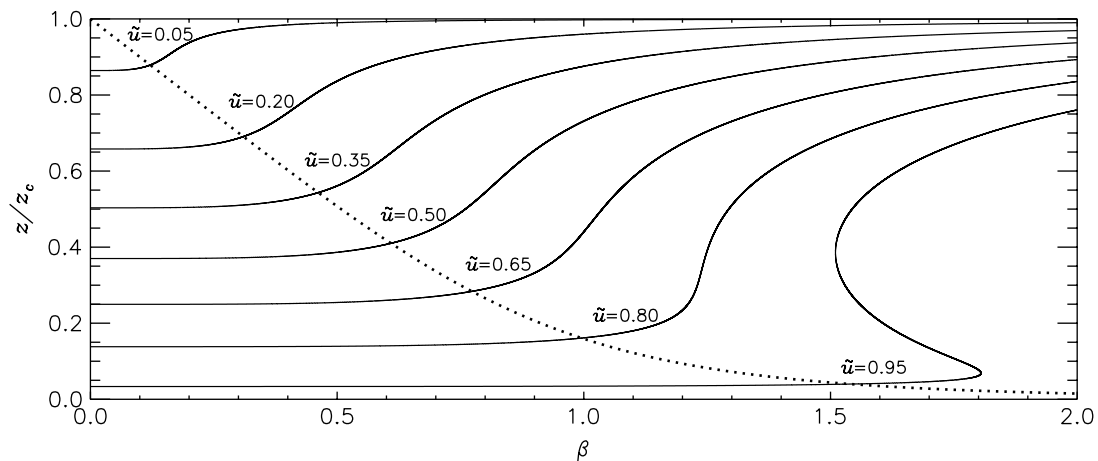


Figure 1. Breaking height \tilde{z}_b as a function of β for different initial amplitudes for fixed \tilde{u} ($= 0.05, \dots, 0.95$ at intervals of 0.15) and height of the maximum wave amplitude (dashed curve). See section 4.1 for a definition of the parameters.

The asymptotic behaviour given by (28) is equivalent to the one obtained with the ray tracing approximation (Figure 3). Moreover, the equivalence of the quasi-optic and ray tracing approximations in the wave amplitude includes superior terms in the asymptotic series; the only difference between the two exact expressions (14) and (27) is that the initial time range σ_ω^{-1} is taken to be zero in the ray tracing.

The initial time range term at (27) is essential to represent the amplitude evolution at short times. In particular, the amplitude maximum in (27) ($\partial_t a(t_M) = 0$) is found at

$$t_M = \left(\frac{Ri}{\sigma_\omega^4} + \frac{Ri^2}{\omega_c^4} \right)^{1/4} - \frac{Ri^{1/2}}{\omega_c}. \tag{29}$$

The height where the wave packet achieves the maximum wave amplitude is obtained from (29) and (12),

$$z_M = z_c \left\{ 1 - \left(\frac{Ri \sigma_\omega^4}{Ri \sigma_\omega^4 + \omega_c^4} \right)^{1/4} \right\} \tag{30}$$

The quasi-optic approximation is able to reproduce both the time and the amplitude of the actual maximum very well as shown in the numerical simulations (section 6). The maxima are found at longer times and higher altitudes for narrower frequency spectra.

The presence of this wave amplitude maximum is also essential to obtain an asymptotic agreement between transient gravity waves in the limit for steady-state waves $\sigma_\omega \rightarrow 0$ and the well-known monochromatic case. Monochromatic waves have the maximum wave amplitude at the critical level where it is unbounded.

The differences between the quasi-optic and ray path approximations are also present in the vertical width evolution (Figure 4). The evolution of the wave packet vertical width in the ray path approximation, (9), is zero at the initial time and then grows monotonically. (All the rays start at the same point at the initial time.) On the other hand the wave packet vertical width in the quasi-optic approximation from (23) results in

$$\Delta z = \Delta z_i \frac{\left[1 + \left\{ \sigma_\omega^2 t / \omega_c (2 + Ri^{-1/2} \omega_c t) \right\}^2 \right]^{1/2}}{(1 + Ri^{-1/2} \omega_c t)^2}. \tag{31}$$

The wave packet vertical width is Δz_i at the initial time and then it diminishes until a minimum is achieved at

$$t_m = \left\{ \left(\frac{Ri}{\omega_c^2} + \frac{\omega_c^2}{\sigma_\omega^4} \right)^{1/2} - \frac{Ri^{1/4}}{\omega_c} \right\}. \tag{32}$$

Interestingly, the time at which the wave packet vertical width minimum (32) is obtained is found at earlier times than the time at which the wave amplitude maximum (29) is achieved. For long times the vertical width under both ray path and quasi-optic approximations tend asymptotically towards a constant.

4. Convective instability analysis

The convective instability threshold is attained when the buoyancy frequency $N^2 = (g/\theta)\partial_z\theta$ (where θ is the potential temperature) becomes zero, i.e.

$$\overline{N^2} = N_0^2 - N_0 |\overline{\partial_z u_1}| = 0, \tag{33}$$

where only the first order is kept and we have used the polarization relation, $N_1^2 = (g/\theta_0)\partial_z\theta_1 = iN_0\partial_z u_1$. As expected, the instability depends only on the phase-averaged vertical shear of the horizontal wind perturbation.

Assuming a slowly varying amplitude (Lighthill, 1978), the instability condition (33) is reduced to

$$1 - \frac{|m_c|a}{N_0} = 0. \tag{34}$$

Equation (34) shows that the threshold depends on the wave amplitude and the vertical wavenumber of the wave packet. This condition determines the minimum time at which the threshold is reached.

Since wave amplitude decreases and vertical wavenumber increases for long times, the asymptotic behaviour determines if the convective threshold is reached. The asymptotic value of the vertical wavenumber from (26) is

$$m_{c,t \rightarrow \infty} = m_{ic} Ri^{-1/2} \omega_c t. \tag{35}$$

Taking the asymptotic value of wave amplitude (28) and vertical wavenumber (35), the buoyancy frequency squared for long times is

$$\overline{N^2} = N_0^2 \left\{ 1 - k_f Ri^{-1/2} \frac{\widehat{u}_\omega}{\sigma_\omega} (\omega_c t)^{1/2} \right\}. \tag{36}$$

As vertical wavenumber increases linearly with time while the wave amplitude decreases as the square root of time, then the phase averaged vertical shear of the horizontal perturbation increases with time near the critical region. Therefore the wave packet will reach the convective threshold. The nature of this convective instability is essentially different from the picture of a quasi-monochromatic wave, where very large amplitudes (wave energy densities) are reached. On the contrary the convective instability given by (36) in a highly transient wave is reached at long times with small amplitudes and high vertical wavenumbers.

Under the quasi-optic approximation, (27) shows that the wave packet reaches a wave amplitude maximum before attaining the asymptotic behaviour. Therefore depending on the parameters of the wave packet, the flow will become convectively unstable either before the wave amplitude maximum or before the vertical wavenumber maximum. Furthermore, we expect that the physical mechanisms involved in these two cases may be different.

The maximum wave amplitude found with quasi-optic approximation occurs at longer times for smaller σ_ω .

Indeed at the limit of monochromatic waves, $\sigma_\omega \rightarrow 0$, the wave amplitude maximum is located at the critical level so that the quasi-optic approximation shows a completely agreement with monochromatic waves when $\sigma_\omega \rightarrow 0$ as already mentioned. Therefore we expect that the characteristics of the convective instability produced by a wave packet near the maximum wave amplitude are similar to the convective instability produced by a monochromatic wave. This feature will be further analysed through numerical simulations in section 6.

4.1. Convective instability in a linear horizontal wind under the quasi-optic approximation

An expression for the adimensionalised breaking altitude $\tilde{z}_b = z_b/z_c$ may be obtained using the convective instability condition, (34), with the wave amplitude given by (27) (which is expressed as a function of z through (26)),

$$\beta^4 = \frac{\tilde{u}^4 - (1 - \tilde{z}_b)^6}{(1 - \tilde{z}_b)^2 (\tilde{z}_b^2 - 2\tilde{z}_b)^2}, \tag{37}$$

where $\tilde{u} = \hat{u}_\omega(\omega_c/k_f)^{-1}$ is the wave amplitude adimensionalised by the phase speed of the central mode and $\beta = Ri^{1/4}\sigma_\omega\omega_c^{-1}$ is the adimensionalised spectral width (weighted by $Ri^{1/4}$).

In the case of a monochromatic wave, $\beta = 0$, the breaking height is given by

$$\tilde{z}_{b \beta \rightarrow 0} = 1 - \tilde{u}^{2/3}, \tag{38}$$

the depth of the critical layer is $1 - \tilde{z}_{b \beta \rightarrow 0} = \tilde{u}^{2/3}$ so that the classical monochromatic result is recovered in this limit. Besides, using (12) and (38) we recover the time limit of linear theory (e.g. Brown and Stewartson, 1980):

$$\omega_c t < Ri^{1/2} (\tilde{u}^{-2/3} - 1), \tag{39}$$

At the other extreme, for a highly transient wave ($\beta \rightarrow \infty$) the wave amplitude goes as

$$\tilde{z}_{b \beta \rightarrow \infty} = 1 - \frac{\tilde{u}^2}{\beta^2}. \tag{40}$$

The breaking height in this limit is the critical level of the central mode. In other words, the highly transient wave will break very close to the critical level of the central mode where the vertical wavenumber is large and the wave amplitude is very small. The nonlinear terms become significant for times longer than

$$\omega_c t = Ri^{1/2} (\beta^2 \tilde{u}^{-2} - 1). \tag{41}$$

In this case, the time limit depends on the spectral width; it is very large for broad spectra.

The breaking height as a function of the transient parameter, β , is shown in Figure 1 for a fixed \tilde{u} . As β grows, we find three breaking regimes:

- I For small β , transient waves break before they reach the maximum amplitude. In this case the breaking amplitude is practically the one given by the monochromatic case (38).
- II For β in the medium range, transient waves break just after they reach the maximum amplitude. The breaking altitude is higher than that given by the monochromatic case.
- III For large β , transient waves break near the critical level of the central mode. This regime represents the highly transient and low initial amplitude cases. This is the only one found in the ray path approximation.

For $\tilde{u} > 2^{-1/4}$, regimes II and III are not present because the curves for a fixed β value contain three solutions. In these cases, the smallest \tilde{z}_b must be interpreted as the breaking height.

The physical processes involved in the dissipation of these so-called breaking regimes are probably different. If the convective instability threshold is reached before the maximum amplitude height, i.e. for waves in the regime I, we expect an abrupt wave breakdown and the subsequent turbulence generation. For waves in regime III, the time to reach the convective instability is longer than for waves in regime I, the wave amplitude at the threshold is very small and the vertical shear induced by the wave is very large so that diffusive processes may

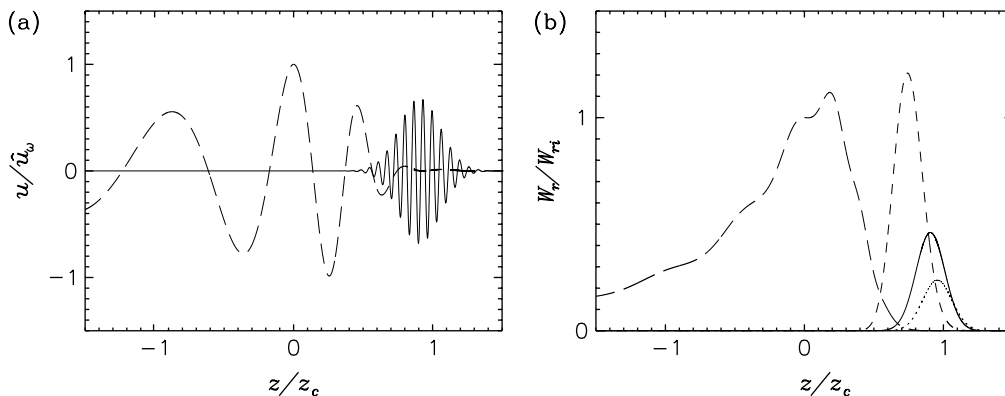


Figure 2. (a) Profile of the horizontal velocity perturbation obtained with the numerical model for a wave packet at $t = 0$ (dashed line) and $t = 12$ h (solid curve) with $\omega_c = 0.10N_0$ and $\sigma_\omega = 0.15\omega_c$ propagating in a background flow defined by $Ri = 100$. (b) Wave energy density at $t = 0$ (long dashed), 4 h (dashed), 12 h (continuous) and 24 h (dotted).

play a more important role in this case. Waves in regime II are in the transition region so that both turbulence generation and diffusive processes may be important to represent their dissipation.

Two extreme wave breaking regimes have already been found by Winters and D’Assaro (1989) in nonlinear numerical simulations of transient wave packets propagating in a shear flow. They found two gravity wave packet evolutions depending on the initial wave amplitude. In a large-amplitude case-study, there is an abrupt breakdown. In the small-amplitude case, the packet is completely absorbed by the mean flow without breaking during its whole life cycle. Lin *et al.* (1993) also find that small-amplitude wave packets do not break; regrettably small amplitude cases are not shown in that work. Even though Wurtele *et al.* (1996) examined a different configuration (inertia critical levels for orographic waves with a horizontal wavenumber spectrum), they also found two wave regimes which depend on the width of the horizontal wavenumber spectrum, in agreement with the results found in the present case for the frequency spectrum. In the context of Figure 1, the two cases examined by Winters and D’Assaro (1989) are two \tilde{u} values for a fixed β ; on the other hand the two cases presented by Wurtele *et al.* (1996) may be thought as two β values for a fixed \tilde{u} .

5. Numerical model

In order to evaluate the theoretical results and to find the range of validity of the different approximations, two sets of numerical simulations were performed with just representative values of the background flow and gravity wave packet characteristics. This numerical study does not pretend to be an exhaustive simulation of realistic situations but an idealised numerical case to be compared with the theoretical results.

The simulations were performed using the numerical model described in detail in Pulido (2005). The model reproduces the evolution of an arbitrary disturbance in a shear wind by solving numerically the Taylor – Goldstein equation in the spectral space followed by a transformation to the physical space.

For each mode in the spectral space, the numerical model solves the Taylor – Goldstein equation and obtains the component of the horizontal velocity ($u(\omega, z)$) as a function of height. The Taylor – Goldstein equation is represented by two first-order differential equations which are solved using the fourth-order Runge – Kutta scheme with adaptive stepsize (Press *et al.* 1992). Once all the spectral components are obtained, they are Fourier transformed to the physical space to obtain $u(z, t)$. As in the theoretical development, we assume that the disturbance is periodic in x .

At $z = 0$, the wave packet modes conform to a Gaussian spectrum so that

$$u(\omega, z = 0) = \frac{\hat{u}_\omega}{\sigma_\omega} \exp \left\{ \frac{-(\omega - \omega_c)^2}{2\sigma_\omega^2} \right\}, \tag{42}$$

where ω_c is the central frequency and σ_ω is the frequency spectral width.

The background is given by a constant buoyancy frequency N_0 and a horizontal wind

$$u_0(z) = \frac{N_0}{Ri^{1/2}} z, \tag{43}$$

where Ri is the background Richardson number. In all cases we take $N_0 = 0.02 \text{ s}^{-1}$ as a representative value.

The numerical experiments were performed from a lower boundary at $z = 0$ to the upper boundary at $z = 3 Ri^{1/2} \omega_c (N_0 k_f)^{-1}$. The radiation condition is imposed in order to keep only upward propagating waves. When the envelope of the wave packet is examined at the initial time, the lower boundary is located at $z = -3\Delta z_i$. The vertical resolution was set at 2 m and the frequency resolution at $10^{-4} \sigma_\omega$.

6. Numerical simulations

Figure 2(a) shows the wave profile at the initial time and at $t = 12 \text{ h}$. At the initial time, the wave packet is quite extended in altitude; because of this the vertical wavenumber and wave amplitude changes due to background wind changes are evident inside the wave

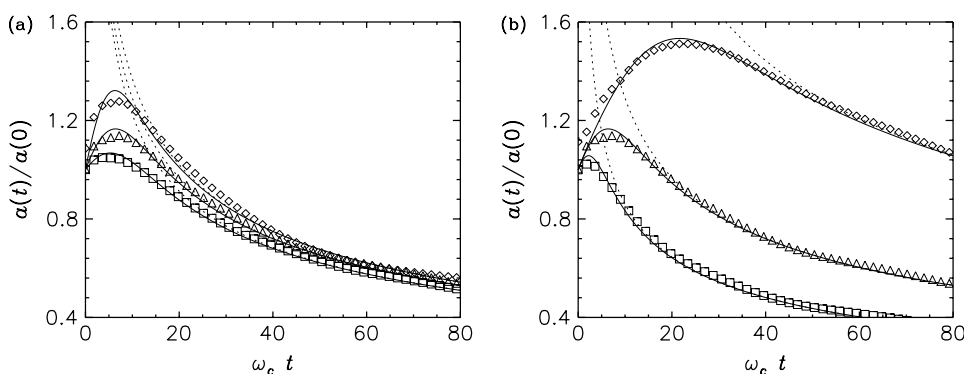


Figure 3. Evolution of the wave amplitude for (a) a wave packet with $\sigma_\omega = 0.1\omega_c$ and different background flows $Ri = 25$ (\diamond), $Ri = 100$ (Δ) and $Ri = 400$ (\square), (b) a background flow given by $Ri = 100$ and for different spectral widths $\sigma_\omega = 0.05\omega_c$ (\diamond), $0.10\omega_c$ (Δ) and $0.15\omega_c$ (\square). The quasi-optic approximation (27) is represented by solid curves and ray path approximation (14) by dashed curves.

envelope. As time goes on, the wave envelope is more compact and the vertical wavenumber increases so that the wave packet is more symmetric and the modulated wave hypothesis (i.e. the envelope width must be composed of many wavelengths) is more clearly satisfied as the transient wave propagates towards the critical region.

The evolution of the wave energy density shows that the wave packet tends towards a Gaussian shape in altitude (Figure 2(b)) so that the wave packet vertical width and the maximum wave amplitude are clearly defined for long times. The wave packet width evolution focuses at short times and then it remains rather constant, although wave amplitude continues to diminish because the intrinsic frequency diminishes monotonically with time (6).

Numerical experiments with different Richardson numbers were performed; the evolution of the wave amplitude is shown in Figure 3(a). We found out that the smaller Richardson number, the larger wave amplitude maximum. This effect is well reproduced by the quasi-optic approximation. Furthermore the wave amplitude does not depend on Richardson number at long times as both quasi-optic and ray path approximations predict.

There are two subtle differences between the numerical experiments and the quasi-optic approximation. The case for small Richardson number (represented by diamonds in Figure 3(a)) presents differences at $t = 0$. These differences may be traced back to the wave energy density profile at $t = 0$ shown in Figure 2(b). This profile contains the maximum amplitude at a higher altitude than $z = 0$; this effect is due to the $(m/m_i)^{1/2}$ factor in each component of the solution. Although the level of perfect constructive interference is at $z = 0$, the $(m/m_i)^{1/2}$ factor produces a larger wave amplitude at higher altitudes. As already mentioned, these effects are most evident for short times (because the wave packet is rather extended in height) and also for small Richardson numbers (because the $(m/m_i)^{1/2}$ changes with height are larger).

The other difference between the analytical prediction (27) and the numerical experiments is a small oscillation that appears in the numerical simulations for long times, particularly for large Richardson number. A set of

numerical experiments with different vertical resolutions shows that the amplitude of the oscillation is reduced for higher vertical resolution (not shown).

A second set of numerical experiments was designed to examine the dependencies of the wave packet spectral width (σ_ω) in order to evaluate the tendencies found in the theoretical development. The asymptotic long-time decay of the amplitude depends on the wave packet width: the broader the spectral width, the smaller the wave amplitude (Figure 3(b)). Furthermore, the maximum amplitude shifts towards longer times for narrower spectral width. This behaviour is also well captured by the quasi-optic approximation.

The evolution of the wave packet vertical width for the experiments with different Ri is shown in Figure 4(a). The vertical width in the numerical experiments is defined to be half of the height difference between the levels where the wave energy density decays to e^{-1} of the maximum amplitude. The wave packet narrows at short times, then the wave packet width grows until it reaches an asymptotic constant value at long times. The correspondence between the theoretical predictions from the quasi-optic approximation and the numerical experiments is remarkable at both short and long times. On the other hand, the ray path approximation reproduces the width evolution for long times, but for short times the ray path width goes to zero.

The asymptotic vertical width is longer for larger Richardson number. This effect is directly related to the spectral distribution of the modes contained in the wave packet. Since each component of the wave packet must reach its own critical level, we expect that the vertical width for long times must be related to the altitude range formed by the critical levels of the different components of the wave packet. For a linear background wind, the critical level for a mode with frequency ω is defined as $z_{c\omega} = \omega(k\partial_z u_0)^{-1}$ so that the asymptotic vertical width for long times is

$$\Delta z(t \rightarrow \infty) = \frac{\sigma_\omega}{k_f \partial_z u_0} = \frac{Ri^{1/2} \sigma_\omega}{N_0 k_f}. \tag{44}$$

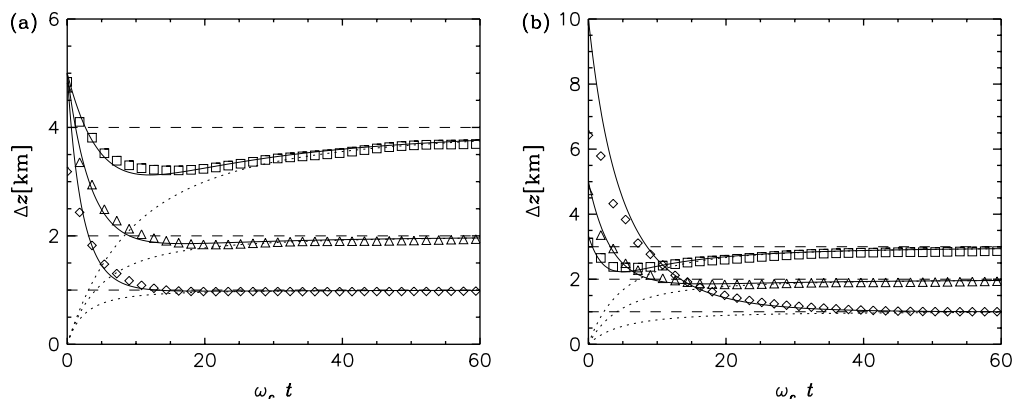


Figure 4. Evolution of the vertical width for (a) wave packets with an initial spectral width of $\sigma_\omega = 0.2\omega_c$ and different Ri , and (b) wave packets propagating in a background with $Ri = 100$ and different σ_ω . The range given by (44) is represented by dashed curves. Other conventions are as in Figure 3.

The so-called critical region may be identified as this height range. This inferred asymptotic wave packet vertical width, (44), agrees for long times with the one obtained analytically in (31) and the numerical experiments (Figure 4(a)).

As expected from (44), the asymptotic vertical width of the wave packet depends linearly on the spectral width σ_ω . Figure 2(b) shows the vertical width evolution corroborating the linear dependence of the asymptotes. There are some differences between the quasi-optic approximation and the numerical simulations at short times for the small σ_ω case; these differences are again related to the extended asymmetric envelope found at the initial time (Figure 3(b)). Note that extended envelopes are very sensitive to the decay rate criterion (the e^{-1} factor) used to define the wave packet range in the numerical simulations.

Our results show that both the wave packet range and the wave action density (from (5)) tend to a constant value for long times. These features are different from the asymptotic tendencies obtained by Grimshaw (1975). The small-amplitude inviscid case examined by Grimshaw presents a wave packet vertical width that goes to zero for long times and thus a wave action density that grows indefinitely as the wave packet propagates towards the critical level. As already mentioned, we take into account the spectral distribution of the wave packet in frequency; each mode possesses a different critical level (instead of only one), forming the so-called critical region. This is the key difference between Grimshaw (1975) and the present study.

The evolution of the buoyancy frequency for the two sets of experiments, for different Richardson numbers and for different spectral widths, are shown in Figure 5. Again the quasi-optic approximation shows good agreement with the numerical results, with the exception of the two problems already found for both the amplitude and width evolution. The cases for small Richardson number (Figure 5(a)) and small spectral width (Figure 5(b)) present negative values for long times; these features are shown for completeness of the curves, since nonlinear processes are thought to be activated near the convective instability threshold. The cases for large Richardson

number and broad frequency spectrum do not reach the convective instability threshold even for the very long times considered in Figure 5. Lin *et al.* (1993) through nonlinear numerical experiments found that the larger the Richardson number, the longer is the time taken to reach the convective instability threshold in agreement with the present linear results. Although wave packets in large Richardson numbers will undoubtedly reach the threshold, we do not expect the linear inviscid approach is valid for such long times. A diffusive process must be acting which may dissipate the transient wave before it reaches the convective instability threshold (Winters and D'Assaro, 1989).

7. Conclusions

Two techniques are applied to examine a transient gravity wave that is propagating towards the critical region. The application of a ray tracing technique is a complement to applications that focus on orographic waves (Broad, 1999). In this work, instead of fixing the absolute frequency, we work under the wave packet assumptions in the frequency spectrum, that is, the central absolute frequency and frequency width are considered parameters. Ray tracing does not reproduce the behaviour found in the wave amplitude for short times. The quasi-optic approximation has a remarkably good performance for short times and long times.

Using the quasi-optic approximation we find three 'breaking' regimes for gravity wave packets that are propagating towards their critical regions. Quasi-steady wave packets with large initial amplitudes attain the convective threshold at some level below the height of maximum wave amplitude (30). This breaking regime is similar to the monochromatic wave case. On the other hand, if the initial wave amplitude is not large enough and the wave packet is highly transient, it will not reach the convective threshold before the maximum wave amplitude is achieved. In this case the convective threshold is achieved for much longer times near the critical region, the amplitude of the wave packet is small and the vertical wavenumber is large at the breaking

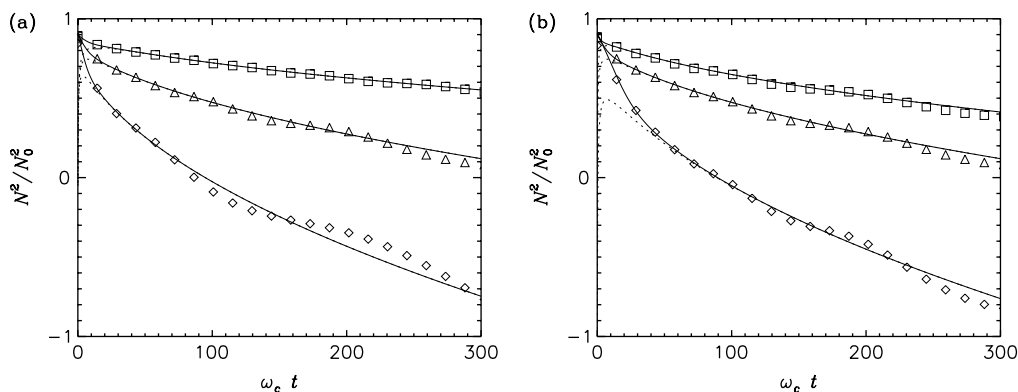


Figure 5. Evolution of the buoyancy frequency (33) for (a) different Richardson numbers and (b) different spectral widths. Conventions are as in Figure 3.

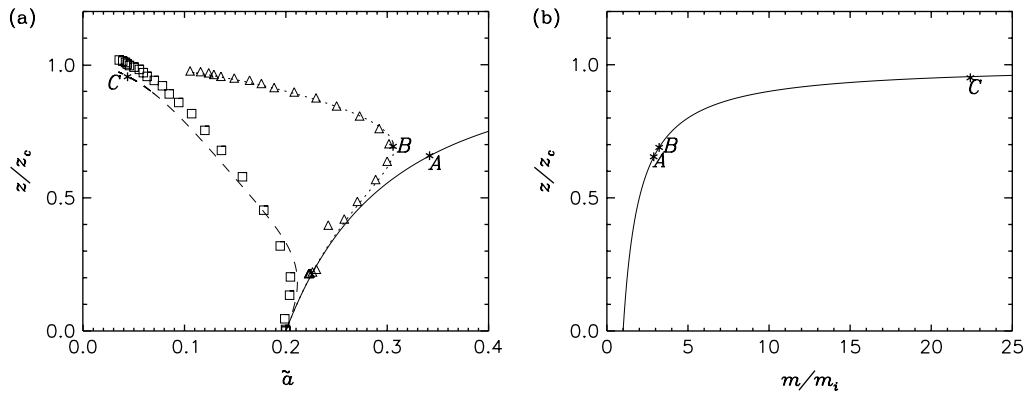


Figure 6. (a) Wave amplitude $\tilde{a} = a(\omega_c/k_f)^{-1}$ as a function of altitude for $\tilde{u}_\omega = 0.2$, $Ri = 100$. The spectral width is $\sigma_\omega = 0.30\omega_c$ (dashed curve), $\sigma_\omega = 0.15\omega_c$ (dotted curve) and the monochromatic case $\sigma_\omega \rightarrow 0$ (solid curve). (b) Vertical wavenumber as a function of altitude. The letters A, B and C in the curves represent the height of breaking for $\sigma_\omega \rightarrow 0$, $\sigma_\omega = 0.15\omega_c$ and $\sigma_\omega = 0.30\omega_c$, respectively.

height. The third regime is a transition regime where both amplitude and vertical wavenumber are important to produce the dissipation of the wave.

To illustrate this result, Figure 6(a) shows the wave amplitude as a function of height for two transient waves and for the monochromatic case. For waves with a narrow spectral distribution in frequency, the breaking height is close to the monochromatic breaking height; the amplitude is also similar although slightly smaller than the monochromatic case. The most transient case does not reach convective instability as the wave amplitude grows so that the threshold is reached near the critical level of the central mode. The ‘breaking’ amplitude is much smaller in this case. Furthermore, the vertical wavenumber for the transient case is much larger than for the monochromatic case (Figure 6(b)). This fact also suggests that we must take into account diffusive processes and viscosity in order to represent correctly the dissipation of highly transient waves.

The processes involved in the gravity wave – critical level interactions are fully nonlinear (e.g. Fritts, 1984). The nonlinear terms in the equations become important in the so-defined critical layer for a sufficiently long time while they are negligible outside it (Brown and Stewartson, 1980). As ray path and quasi-optic techniques are based on linear wave theory, they can only be used outside the critical layer. The complex physical processes involved in wave breaking inside the critical layer are beyond the scope of these linear techniques. Indeed our long-time predictions of wave evolution are shown only for illustrative purposes; wave amplitudes for long times are likely to be affected by both nonlinear and diffusive processes.

One may also wonder to what extent the breaking height estimated under linear wave theory may be realistic. There are a number of numerical nonlinear studies that evaluate the scope of linear wave theory with encouraging results. Dörnbrack and Nappo (1997) found good agreement between the linear breaking height and the breaking height found in numerical simulations. (The configuration was taken to reproduce the results of a laboratory experiment of gravity wave breaking.) The

nonlinear numerical simulations performed by Winters and D’Assaro (1989) suggest that the entire life cycle of small-amplitude wave packets is governed by linear wave theory. Prusa *et al.* (1996) for a constant background flow also found that the actual breaking height was predicted precisely by linear wave theory, moreover the vertical and horizontal extension predicted by linear theory were also in good agreement with the numerical simulation.

Actual gravity wave parametrizations usually apply only one criterion of breaking independently of the wave characteristics, with the exception of Warner and McIntyre (1996) who apply an empirical criterion in the spectral space. This work, in agreement with the Winters and D’Assaro results, suggests that a more realistic gravity wave parametrization should consider the wave characteristics (particularly a measure of the transiency of the disturbances, say σ_ω , and the spectral amplitude) in order to discern whether transient waves dissipate by overturning or by diffusive processes.

Acknowledgment

We thank Prof. J. Thurnbun for calling our attention to Broad’s work and the reviewers for helpful comments.

References

- Booker J, Bretherton F. 1967. The critical layer for internal gravity waves in a shear flow. *J. Fluid. Mech.* **27**: 513–539.
- Bretherton F, Garrett C. 1968. Wavetrains in inhomogeneous moving media. *Proc. R. Soc. A* **302**: 529–554.
- Broad A. 1999. Do orographic gravity waves break in flows with uniform wind direction turning with height? *Q. J. R. Meteorol. Soc.* **125**: 1695–1714.
- Brown SN, Stewartson K. 1980. On the nonlinear reflexion of a gravity wave at a critical level. Part 1. *J. Fluid. Mech.* **100**: 577–595.
- Dörnbrack A, Nappo CJ. 1997. A note on the application of linear wave theory at a critical level. *Boundary-Layer Meteorol.* **82**: 399–416.
- Fritts DC. 1984. Gravity wave saturation in the middle atmosphere: A review of theory and observations. *Rev. Geophys.* **22**: 275–308.
- Grimshaw R. 1975. Nonlinear internal gravity waves and their interaction with the mean wind. *J. Atmos. Sci.* **32**: 1779–1793.
- Hines CO. 1991. The saturation of gravity waves in the middle atmosphere. Part II: Development of Doppler-spread theory. *J. Atmos. Sci.* **48**: 1361–1379.
- Holton J. 1982. The role of gravity wave induced drag and diffusion in the momentum budget of the mesosphere. *J. Atmos. Sci.* **39**: 791–799.

- Jones W. 1967. Propagation of internal gravity waves in fluids shear flow and rotation. *J. Fluid Mech.* **30**: 439–448.
- Lighthill MJ. 1978. *Waves in fluids*. Cambridge University Press: Cambridge, UK.
- Lin CL, Ferziger JH, Koseff JR, Monismith SG. 1993. Simulation and stability of two-dimensional internal gravity waves in a stratified shear flow. *Dyn. Atmos. Oceans* **19**: 325–366.
- Ostrovsky LA, Potapov AI. 1999. *Modulated waves. Theory and applications*. Johns Hopkins University Press: Baltimore, USA.
- Palmer TN, Shutts GJ, Swinbank R. 1986. Alleviation of a systematic westerly bias in general circulation and numerical weather prediction models through an orographic gravity wave drag parametrization. *Q. J. R. Meteorol. Soc.* **112**: 1001–1039.
- Piani C, Norton WA, Stainforth DA. 2004. Equatorial stratospheric response to variations in deterministic and stochastic gravity wave parameterizations. *J. Geophys. Res.* **109**: D14101.
- Press WH, Flannery BP, Teukolsky SA, Vetterling WT. 1992. *Numerical recipes in FORTRAN: The art of scientific computing*. Cambridge University Press: Cambridge, UK.
- Prusa JM, Smolarkiewicz PK, Garcia RR. 1996. Propagation and breaking at high altitudes of gravity waves excited by tropospheric forcing. *J. Atmos. Sci.* **53**: 2186–2216.
- Pulido M. 2005. On the Doppler shifting effect in an atmospheric gravity wave spectrum. *Q. J. R. Meteorol. Soc.* **131**: 1215–1232.
- Shutts GJ. 1998. Stationary gravity-wave structure in flows with directional wind shear. *Q. J. R. Meteorol. Soc.* **124**: 1421–1442.
- Warner CD, McIntyre ME. 1996. On the propagation and dissipation of gravity wave spectra through a realistic middle atmosphere. *J. Atmos. Sci.* **53**: 3213–3235.
- Winters KB, D'Assaro EA. 1989. Two-dimensional instability of finite amplitude internal wave packets near a critical level. *J. Geophys. Res.* **94**: 12709–12719.
- Wurtele M, Datta A, Sharman R. 1996. The propagation of gravity-inertia waves and lee waves under a critical level. *J. Atmos. Sci.* **53**: 1505–1523.